Activated carbon as a carrier for amorphous drug delivery: Effect of drug characteristics and carrier wettability

Nikhila Miriyala [a] , Defang Ouyang [b], Yvonne Perrie [c], Deborah Lowry [d], Daniel J. Kirby [a*]

[a] *Aston Pharmacy School, School of Life and Health Sciences, Aston University, Birmingham, B4 7ET, United Kingdom.*

[b] *State Key Laboratory of Quality Research in Chinese Medicine, Institute of Chinese Medical Sciences (ICMS), University of Macau, Macau, China.*

[c] *University of Strathclyde, Glasgow, United Kingdom*

[d] *School of Pharmacy and Pharmaceutical Sciences, Ulster University, United Kingdom*

*Corresponding author. Aston Pharmacy School, Aston University, Birmingham, UK, B47ET. Tel: +44(0)1212043006 Email: d.j.kirby1@aston.ac.uk

Abstract

Recent research on porous silica materials as drug carriers for amorphous and controlled drug delivery has shown promising results. However, due to contradictory literature reports on toxicity and high costs of production, it is important to explore alternative safe and inexpensive porous carriers. In this study, the potential of activated carbon (AC) as an amorphous drug carrier was investigated using paracetamol (PA) and ibuprofen (IBU) as model drugs. The solution impregnation method was used for drug loading, with loading efficiency determined by UV spectroscopy and drug release kinetics studied using USP II dissolution apparatus. The physical state of the drug in the complex was characterised using differential scanning calorimetry and X-ray diffractions techniques, whilst sites of drug adsorption were studied using Fourier transform infrared spectroscopy and N_2 adsorption techniques. In addition, the cytotoxicity of AC on human colon carcinoma (Caco-2) cells was assessed using the MTT assay. Results presented here reveal that, for PA/AC and IBU/AC complexes, the saturation solubility of the drug in the loading solvent appears to have an effect on the drug loading efficiency and the physical state of the drug loaded, whilst drug release kinetics were affected by the wettability of the activated carbon particles. Furthermore, activated carbon microparticles exhibited very low cytotoxicity on Caco-2 cells at the concentrations tested (10-800 µg/mL). This study, therefore, supports the potential of activated carbon as a carrier for amorphous drug delivery.

Keywords: Activated carbon, Amorphous drug delivery, Paracetamol, Ibuprofen, Oral drug delivery, Porous carrier

Chemical compounds studied in this article

Paracetamol (PubChem CID: 1983); Ibuprofen (PubChem CID: 3672); Ethanol (PubChem CID: 702); Sodium dodecyl sulphate (PubChem CID: 3423265)

Abbreviations: AC, activated carbon; PA, paracetamol; IBU, ibuprofen; PA/AC phy mix, physical mixture of paracetamol and activated carbon; PA/AC complex, paracetamol loaded activated carbon ; IBU/AC phy mix, physical mixture of ibuprofen and activated carbon; IBU/AC complex, ibuprofen loaded activated carbon;

1. Introduction

The effectiveness of an oral dosage form depends on the bioavailability of the drug, which in turn depends on its solubility and dissolution rate. However, more than 90% of active pharmaceutical ingredients have oral bioavailability issues [1] and about 40% have solubility and dissolution limitations [2]. With a limited number of compounds possessing drug like properties, it is important to develop effective techniques to improve the solubility and dissolution behaviour of poorly water-soluble drugs [3].

One of the many solubility enhancing techniques includes conversion of a crystalline drug to an amorphous form; the dissolution rate of amorphous forms of drugs is markedly better than the crystalline form, especially in drugs with high crystal energy [4,5]. The absence of molecular order in amorphous forms of drugs allows greater motion of molecules, resulting in higher solubility, which plays a crucial role in achieving optimum bioavailability. However, amorphous forms have poor stability and often tend to convert back to crystalline forms [6].

Several studies have been performed to develop stabilising strategies for the amorphous form of drugs [7,8], with loading of drugs into porous materials showing great potential [9]; the interactions between the carrier and the adsorbed drug, as well as the small pore size of the carriers, restricts the crystallisation of the drug. Various types of porous materials have been studied as drug carriers for amorphous drug delivery, although there are still many limitations hindering the technique, such as complexity of production, low drug loading efficiency, high production costs and safety concerns, as highlighted in Table 1. Hence, it is important to explore porous materials that can address the aforementioned issues.

This current study investigates the application of activated carbon (AC) as a drug carrier for amorphous drug delivery. AC is inexpensive, commercially available, non-toxic and has a high surface area to volume ratio, which can favour development of an effective, inexpensive and safe carrier for oral drug delivery. AC is produced from a variety of materials rich in carbon (e.g. coal, wood, peat etc.), by either steam activation or chemical activation. Activation develops porosity in the carbon and the pore size is affected by the process of activation [28]. AC consists of a three-dimensional interconnected pore structure, with micropores (pore width <2 nm), mesopores (pore width 2-50 nm) and macropores (pore width >50 nm) [29].

AC is extensively used in drinking water treatment and is also clinically used as an antidote to remove poisonings [30–32], whilst several studies have explored its use for various clinical applications, as noted in Table 2.

In this study, the solution adsorption method was used for drug loading in to AC, using paracetamol (PA) and ibuprofen (IBU) as model drugs with different saturation solubilities in ethanol, in order to determine the effect of solubility on drug loading.

2. Experimental section

2.1. Materials

Activated carbon DARCO® G-60 was purchased from Sigma Aldrich, UK. Crystalline paracetamol powder was obtained from GlaxoSmithKline, UK. Crystalline ibuprofen powder was purchased from SLS, UK. Ethanol, dimethyl sulfoxide, sodium dodecyl sulphate, sodium dihydrogen phosphate and disodium hydrogen phosphate were purchased from Fisher, UK. Caco-2 cells were purchased from ATCC. Dulbecco's Modified Eagle's Medium, foetal bovine serum, trypsin-EDTA solution, anti-mycotic solution, Hank's balanced salt solution, MTT dye, phosphate buffered saline and trypan blue were purchased from Sigma Aldrich, UK.

2.2. Characterisation of activated carbon

2.2.1. Particle size distribution

Particle size analysis of activated carbon was performed using laser diffraction (HELOS, Sympatec GmbH, Germany). 25 mg of carrier was dispersed in 200 mL of ethanol and was analysed for particle size in the measuring range of 0.1 to 500 µm.

2.2.2. Cell culture and Cytotoxicity assay

Cells were cultured in Dulbecco's Modified Eagle's Medium (DMEM, with 4500 mg/L glucose, L-glutamine, sodium pyruvate, sodium bicarbonate, amino acids and vitamins) with 10% FBS in culture flasks and incubated at 37 °C in an atmosphere of 5% CO_2, and the medium was changed every 2 days. Cells were sub-cultured when they reached about 60% confluency. Studies were performed on cells between passages 100 and 120.

The cell suspension was diluted to achieve a density of 10^4 cells/mL using DMEM. Cell suspension was added to 96 well plates at 100 µL per well, such that each well had a density of 1000 cells. The cells were incubated for 24 hours. The spent medium was then removed and the suspensions with different concentrations of carrier (10-800 µg/mL) were added to 96-well plates at 100 µL per well and incubated for a further 24 hours. Caco-2 cells without carrier suspension were used as a control. Morphology of cells was observed under light microscope. The spent medium was removed after 24 hours of incubation. 100 µL of fresh medium and 20 µL of 5mg/mL MTT in PBS solution was added to each well and incubated for 4 hours. After 4 hours, the medium containing MTT was removed and replaced with 100 µL DMSO. The absorbance of the resulting formazan solution was determined at 492 nm on a SynergyTM HT microplate reader (Biorad, USA).

2.3. Preparation of drug loaded activated carbon and determination of drug loading efficiency

Solution adsorption is a commonly used method for drug loading in to a porous carrier, where the carrier is immersed in a saturated drug solution for a specific duration [39]. In this study, drug was dissolved in 10 mL of ethanol to obtain a saturated drug solution at 20 °C (saturation solubility of paracetamol and ibuprofen at 20 °C is 190.61 g/kg and 886.5 g/kg of ethanol, respectively [40,41]). 1 g of activated carbon was added to the drug solution and the suspension was stirred at 25 °C on a hot plate stirrer for 24 hours. The dispersion was centrifuged at 1500 rpm and the supernatant was collected for further analysis. The sediment was allowed to dry in an oven at 40 °C for 24 hours.

Drug loading efficiency was determined by UV spectroscopy (Jenway, UK). 50 mg of drug/carrier complex was added to 50 mL of ethanol and was stirred for 24 hours at 25 °C. The solution was filtered and the concentration of the drug in the filtrate was determined. Loading efficiency of activated carbon was calculated using Eq. (1) as follows:

$$Loading\ efficiency\ (\%) = \frac{weight\ of\ the\ drug\ in\ complex}{total\ weight\ of\ \ complex} \times 100 \qquad (1)$$

2.4. Characterisation of drug loaded activated carbon complex

2.4.1. Powdered X-ray diffraction (XRD) analysis

The XRD patterns of the samples were recorded on a D8 ADVANCE diffractometer (Bruker, USA) in the angular range of 10° to 50° (2θ) with a step size of 0.02°, using a Cu–Kα source operated at 30 kV and 30 mA.

2.4.2. Differential Scanning calorimetry (DSC)

Thermal analysis was performed using a Q100 DSC instrument (TA instruments Ltd., UK). 2 mg of sample was weighed and transferred to a Tzero aluminium pan, with the subsequent temperature scan performed at a heating rate of 10 ºC/min under N_2 gas. Percentage crystallinity in the drug loaded carrier was calculated from the melting enthalpy of physical mixture of drug and carrier using Eq. (2) [42] :

$$\frac{Xc(\%)}{Xc°(\%)} = \frac{\Delta Hm}{\Delta Hm°} \qquad (2)$$

Where $Xc(\%)$= percentage of crystallinity in the drug/carrier complex. $Xc°(\%)$ = percentage of crystallinity in drug/carrier physical mixture and is considered to be 100. ΔHm = melting enthalpy of the drug/carrier complex. $\Delta Hm°$ = melting enthalpy of drug/carrier physical mixture.

2.4.3. Fourier transform infra-red spectroscopy (FTIR)

Spectra were recorded in the range of 500-4000 cm^{-1} using a Nicolet iS5 spectrometer (ThermoFisher Scientific Inc, UK) equipped with iD5 ATR (Attenuated total reflectance) accessory with a laminated diamond crystal at an angle of incidence of 42°. The spectra were obtained at a spatial resolution of 4 cm^{-1} and were an average of 16 scans.

2.4.4. Nitrogen sorption analysis

Nitrogen adsorption isotherms at 77 K were obtained using an ASAP 2420 (Accelerated surface area and porosimetry system, Micrometrics, USA). Activated carbon powder was degassed at 200 °C for 4 hours and drug containing activated carbon was degassed at 40 °C for 24 hours. The specific surface area of the sample was computed using the Brunauer–Emmett–Teller (BET) method in the relative pressure range between 0.01 and 0.9. The pore size distribution of the sample was calculated using nonlinear density functional theory (NLDFT) method, assuming slit shaped pores.

2.4.5. Drug release studies

Drug release from the complex was studied with a USP Type II dissolution apparatus (Erweka GmbH, Germany) using pure crystalline drug (equivalent to the amount of drug in the complex) as a control. Sodium phosphate buffer at either pH 5.8 or pH 7.2, with and without 1% *w/v* sodium dodecyl sulfate (SDS), were used as dissolution media for paracetamol and ibuprofen, respectively. Dissolution was performed at 37 °C with paddle stirring speed of 100 rpm. Samples were withdrawn at specific time intervals and replaced with fresh dissolution medium. The samples were filtered using 0.45 µm syringe filters and analysed using UV spectrophotometry at wavelengths of 257 nm and 264 nm for paracetamol and ibuprofen, respectively.

2.5. Statistical analysis

Statistical analysis was carried out on the data by one way ANOVA, using Graph pad prism software (Version 6.0 for Windows). Statistically significant differences were denoted for p values of less than 0.05.

3. Results and Discussion

3.1. Characterisation of activated carbon

Particle size of the porous carrier is an important characteristic, since, amongst other aspects, it may affect the drug release rate; drug loaded in deeper pores of larger particles will need to travel a longer distance before release [43]. Also, particle size can affect the cytotoxicity, where nanoparticles could result in increased toxicity compared to microparticles due to a higher chance of internalisation by cells [23]. However, internalisation of microparticles (0.1-10 µm) by endocytosis has also been observed [44,45]. Due to the above reasons, determining the particle size and toxicity of activated carbon is crucial.

AC used in this study has a particle size in the range of 0.55- 87.5µm (Fig.1), with nearly 40% of the particles ≤ 10 µm in size, indicating the possibility of internalisation by cells and toxicity. Hence, cell cytotoxicity of activated carbon on Caco-2 cells was evaluated by MTT assay. Although no significant toxicity was observed for concentrations 10-200 µg/mL, significant toxicity was observed for the concentrations ≥ 400 µg/mL ($p \leq 0.05$, one way ANOVA and Dunnett's multiple comparison test) as shown in Fig. 2. The slight toxicity at high concentrations was probably due to adsorption of nutrients in the culture medium by activated carbon particles

[46,47]. Nevertheless, even at the highest concentration (800 µg/mL) tested, the cell viability was still over 80%, suggesting that application of AC with a particle size above 0.55 µm could be safe for oral drug delivery.

3.2. Drug loading into activated carbon

After 24 hours of drying the sediment obtained from centrifugation (Section 2.3), the unloaded/free drug was found to crystallise as a top layer due to the evaporation of the solvent, as shown in Fig.3. The top crystalline layer was removed and analysed for drug content, whilst the bottom layer was, sieved (mesh 150-opening size 104 µm) to remove any aggregates, labelled as drug/carrier complex and analysed for drug loading efficiency (Table 3). During the process of removal of the top crystalline layer, an amount of drug loaded activated carbon was also removed; therefore, the total amount of activated carbon present in the drug/carrier complex is not equal to 1000 mg.

The higher loading efficiency for ibuprofen (IBU) compared to paracetamol (PA) could be attributed to the higher solubility of IBU in ethanol. Although the loading efficiency was higher, the fraction of adsorbed to the unadsorbed drug was lower for IBU compared to that of PA, which could be due to stronger interactions between IBU and ethanol or due to saturation of AC. It was also found that analysis of free drug in the supernatant solution can give a false estimation of drug loading capacity, since it does not consider the top crystalline layer of the sediment.

3.3. Solid state analysis of drug

DSC and XRD techniques were used to detect crystallinity in the drug/carrier complex. DSC can also identify any re-crystallisation of the drug that is initially present in an amorphous state. DSC curves for pure drug, activated carbon, drug/carrier complex and drug/carrier physical mixture are shown in Fig.4 (a) and (b), whilst melting temperature and melting enthalpy obtained are presented in Table 4; the presence of crystalline drug in the drug/carrier complex can be detected from the melting peak of crystalline drug. Pure paracetamol and physical mixture exhibited a melting peak at 169 °C, characteristic of monoclinic Form I paracetamol [48]. Pure ibuprofen and physical mixture exhibited a melting peak at 74.8 °C [49,50], again indicative of crystalline drug. For the drug/carrier complexes, no crystalline drug could be detected in PA/AC complex, whereas crystallinity was detected in IBU/AC complex, possibly as a consequence of the higher drug loading compared to PA/AC complex. Further analysis revealed that the percentage crystallinity in the IBU/AC complex, which was calculated from the melting enthalpy of physical mixture

containing an equal amount of drug as the complex, was found to be about 19% of the total drug present in the IBU/AC complex. These results suggest that using a saturated drug solution for loading is not suitable for all drugs, especially for drugs with high solubility in the respective solvent, and could result in increased crystallinity and reduced uniformity in the drug/carrier complex. Hence, it is important to determine the optimum concentration required in the loading solution for each drug to obtain drug/carrier complexes with no drug crystallinity. Also, it was observed that the melting enthalpy of the drug in the physical mixture was lower than that of the pure drug, which could be attributed to the interactions between AC surface and the drug undergoing the melting process, leading to reduced intermolecular forces in the drug [51,52]. Reduction of enthalpy could also be due to adsorption of drug in to the pores of AC during the process of melting, although the reasons behind this would require further investigation.

The DSC results were also supported by X-ray diffraction studies (Fig.5). XRD patterns of pure IBU and IBU/AC physical mixture samples (Fig.5 (a)) showed characteristic peaks at 11.8°, 16.4°, 17.4°, 20° and 22° (2θ), suggesting the highly crystalline nature of IBU [53,54]. IBU/AC complex also showed a diffraction pattern corresponding to crystalline IBU; however, the peaks at 20° and 22° were less intense, suggesting reduced crystallinity of IBU. XRD patterns (Fig. 5 (b)) of PA and PA/AC physical mixture samples showed characteristic peaks corresponding to crystalline PA at 15.4°, 18.1°, 20.3°, 23.3°, 24.2° and 26.4° [55]. No XRD pattern corresponding to crystalline PA could be detected in the case of PA/AC complex, supporting the DSC results, suggesting that the PA is completely present in an amorphous form, which indicates that PA is effectively loaded in to the pores of AC. However, with IBU/AC complex, crystallinity (19%) was detected, which indicates that IBU is not completely loaded in to the pores of AC and could be present as separate crystals. From the UV analysis, loading efficiency for IBU was found to be 44.4 %, whilst from DSC, 19% of the drug loaded was found to be crystalline, which is equivalent to 122 mg of IBU (total amount of drug in the complex was 643 mg, as shown in Table 3). Therefore, in order to determine the theoretical loading efficiency of IBU into the pores of AC in amorphous state, the amount of crystalline IBU is subtracted from the total IBU loaded, which was determined to be 39%, suggesting that IBU/AC complex with loading higher than this could result in crystallisation of IBU. As such, IBU/AC complex with completely amorphous drug may be achieved by reducing the concentration of IBU in the loading solution, thereby avoiding overloading, although this would require further investigation.

3.4. Sites of drug adsorption

Drug deposited on the external surface of AC can pose a risk of re-crystallisation during storage; as such, FTIR was used to detect any unloaded drug particles or drug deposited on the surface of AC. FTIR spectra of pure drug, drug/carrier physical mixture, and carrier and drug/carrier complex are shown in Fig. 6 (a) and (b). The sloping of spectra in samples containing AC is due to an increase in the absorption by carbon at lower wavenumbers, since the depth of penetration increases at lower wavenumbers [56]. Spectra of paracetamol and physical mixture showed peaks corresponding to an NH amide band stretch at 3320 cm^{-1} and a broad phenolic OH stretch at 3129 cm^{-1}. No significant peaks corresponding to PA were found in the case of PA/AC complex (Fig. 6 (a)). Since the depth of penetration of IR in to the samples is only about 0.2-5 microns, drug deposited in the deeper pores may not be detected [57], which suggests that the paracetamol was loaded in the pores of activated carbon and was absent on external surface of the particles. However, with IBU/AC complex, peaks corresponding to carbonyl CO stretch at 1694 cm^{-1} can be detected, similar to the pure IBU and physical mixture (Fig. 6 (b)), which could be due to the presence of IBU as separate drug crystals or drug adsorbed on the external surface. Results from FTIR studies support the DSC and XRD data, that the drug in PA/AC complex is completely present in the pores of AC in a stable amorphous state. However, in the case of IBU/AC complex, drug is present outside the pores, either deposited on the external surface of AC or as separate crystals.

3.5. In vitro drug release studies

In vitro drug release from the complex was studied using the paddle type dissolution apparatus. Drug release profiles for pure drug and drug/carrier complex are shown in Fig. 7 (a) and (b). Unfavourably, only 54 ± 2.8% (PA/AC) and 61 ± 3% (IBU/AC) of the total drug loaded was released from the drug/carrier complex in sodium phosphate buffer within 10 mins, after which no further drug release was observed. Incomplete drug release from the complex could be due to poor wettability of carbon particles (powder samples floating on the surface of the dissolution medium could be observed). Hence, 1% SDS was added to the dissolution medium to prevent floating of powders; in the presence of SDS, complete drug release was achieved within 10 min for both drug loaded complexes. Indeed, the release rate was higher for PA/AC complex compared to the pure drug, whereas no marked difference was observed for IBU/AC complex, which could be due to the faster release of pure IBU. Both drug loaded complexes in SDS showed complete drug release within 10 minutes irrespective of their individual release rates (Pure PA and Pure

IBU in the presence of SDS achieved complete release within 20 min and 15 min, respectively), which could be due to the stronger influence of the porosity of the AC on the dissolution profiles compared to the drug characteristics, although this would require further investigation to elucidate the mechanisms involved. Compared to the pure crystalline drug, a higher initial release or a burst effect (with and without SDS) and faster complete release (with SDS) were observed for both drug loaded complexes, which could be due to release of drug from superficial pores and the amorphous nature of the drug, respectively. Compared to pure drug, amorphous drug present in the pores of AC has a higher surface area in contact with the dissolution media, which can result in faster release; thus, the drug loaded in to AC, compared to the pure crystalline drug, favoured faster release.

3.6. Porosity analysis of carrier before and after drug loading

Adsorption isotherms and pore size distribution curves are shown in Fig. 8 (a & b), with the data from N_2 sorption studies summarised in Table 5. The adsorption/desorption isotherm of AC exhibited a typical type IV isotherm, with a hysteresis loop characteristic of microporous materials with significant mesoporosity [58]. Unloaded activated carbon particles showed higher surface area and pore volume compared to drug/carrier complex, demonstrating the pore filling by drug molecules in both PA and IBU loaded AC samples. Although the amount of drug loaded in PA/AC complex was markedly lower (Table 3), total pore volume was only slightly higher compared to IBU/AC complex, which could indicate the presence of surface adsorbed or separate, non-associated crystals of IBU. The pore size distribution of pure AC shows the presence of pores in the range of 2-14 nm. Post loading, a reduction in pore size was observed for PA/AC complex, but the general characteristics of pure AC were retained. However, in the case of IBU/AC complex, pores with size > 6 nm were greatly reduced, which could be due to the reduction of pore size from higher drug loading.

4. Conclusion and perspective

Paracetamol and ibuprofen were successfully loaded in to activated carbon, with a drug loading of 20.7 ± 1 % and 44.4 ± 4 % (*w/w)* achieved for PA and IBU, respectively. PA loaded in to activated carbon was completely amorphous, whereas 19% of the IBU loaded in to activated carbon was found to be crystalline, suggesting that the true loading efficiency for amorphous IBU is only 39%. FTIR studies suggested the absence of surface adsorbed drug in PA/AC complex, whereas surface adsorbed drug or separate drug crystals were detected in IBU/AC complex. The

higher loading of IBU and presence of crystallinity in the IBU/AC complex could be due to higher concentration of IBU in loading solution, supporting the theory that the chemical nature of the drug has an effect on the loading efficiency, and the use of a saturated drug solution for drug loading cannot always be recommended. *In vitro* release studies suggested that drug release was complete within 10 min (in the presence of 1% SDS) for both PA/AC complex and IBU/AC complex. The release rate of drug/carrier complex was independent of the characteristic release rate of the pure drug. The low toxicity, high drug loading capacity and ability to stabilise amorphous drug supports the potential of activated carbon as an amorphous drug carrier.

Acknowledgements

This research was partially funded by Aston University through an overseas student scholarship.

References

[1] P. Fasinu, V. Pillay, V.M.K. Ndesendo, L.C. Du Toit, Y.E. Choonara, Diverse approaches for the enhancement of oral drug bioavailability, Biopharm. Drug Dispos. 32 (2011) 185–209. doi:10.1002/bdd.750 C2 - 21480294.

[2] H.D. Williams, N.L. Trevaskis, S.A. Charman, R.M. Shanker, W.N. Charman, C.W. Pouton, C.J.H. Porter, Strategies to Address Low Drug Solubility in Discovery and Development, Pharmacol. Rev. . 65 (2013) 315–499. doi:10.1124/pr.112.005660.

[3] C.A. Lipinski, Drug-like properties and the causes of poor solubility and poor permeability, J. Pharmacol. Toxicol. Methods. 44 (2000) 235–249. doi:http://dx.doi.org/10.1016/S1056-8719(00)00107-6.

[4] B.C. Hancock, G. Zografi, Characteristics and significance of the amorphous state in pharmaceutical systems., J. Pharm. Sci. 86 (1997) 1–12. doi:10.1021/js9601896.

[5] J. Salonen, A.M. Kaukonen, J. Hirvonen, V.P. Lehto, Mesoporous silicon in drug delivery applications, J. Pharm. Sci. 97 (2008) 632–653. doi:10.1002/jps.20999 C2 - 17546667.

[6] L. Yu, Amorphous pharmaceutical solids: preparation, characterization and stabilization, Adv. Drug Deliv. Rev. 48 (2001) 27–42. doi:http://dx.doi.org/10.1016/S0169-409X(01)00098-9.

[7] K.R. Jadhav, S.S. Pacharane, P.P. Pednekar, P.V.K. and V.J. Kadam, Approaches to Stabilize Amorphous Form - A Review, Curr. Drug Ther. 7 (2012) 255–262. doi:http://dx.doi.org/10.2174/1574885511207040004.

[8] R. Laitinen, K. Löbmann, C.J. Strachan, H. Grohganz, T. Rades, Emerging trends in the stabilization of amorphous drugs, Int. J. Pharm. 453 (2013) 65–79. doi:http://dx.doi.org/10.1016/j.ijpharm.2012.04.066.

[9] M. Vallet-Regi, F. Balas, D. Arcos, Mesoporous materials for drug delivery, Angew. Chemie - Int. Ed. 46 (2007) 7548–7558. doi:10.1002/anie.200604488.

[10] J. Salonen, L. Laitinen, A.M. Kaukonen, J. Tuura, M. Björkqvist, T. Heikkilä, K. Vähä-Heikkilä, J. Hirvonen, V.P. Lehto, Mesoporous silicon microparticles for oral drug delivery: Loading and release of five model drugs, J. Control. Release. 108 (2005) 362–374. doi:http://dx.doi.org/10.1016/j.jconrel.2005.08.017.

[11] K.L. Jarvis, T.J. Barnes, C.A. Prestidge, Surface chemistry of porous silicon and implications for drug encapsulation and delivery applications, Adv. Colloid Interface Sci. 175 (2012) 25–38. doi:10.1016/j.cis.2012.03.006.

[12] T. Limnell, Mesoporous silica- and silicon-based materials as carriers for poorly water soluble drugs, University of Helsinki, 2011.

[13] W. Xu, J. Riikonen, V.P. Lehto, Mesoporous systems for poorly soluble drugs, Int. J. Pharm. 453 (2013) 181–197. doi:10.1016/j.ijpharm.2012.09.008.

[14] P. Kinnari, E. Mäkilä, T. Heikkilä, J. Salonen, J. Hirvonen, H.A. Santos, Comparison of mesoporous silicon and non-ordered mesoporous silica materials as drug carriers for itraconazole, Int. J. Pharm. 414 (2011) 148–156. doi:10.1016/j.ijpharm.2011.05.021.

[15] W. Wu, C. Ye, H. Xiao, X. Sun, W. Qu, X. Li, M. Chen, J. Li, Hierarchical mesoporous silica

nanoparticles for tailorable drug release, Int. J. Pharm. 511 (2016) 65–72. doi:10.1016/j.ijpharm.2016.06.133.

[16] X. Zhang, M. Cresswell, Chapter 4 - Silica-Based Amorphous Drug Delivery Systems, in: X. Zhang, M. Cresswell (Eds.), Inorg. Control. Release Technol., Butterworth-Heinemann, Boston, 2016: pp. 93–137. doi:http://dx.doi.org/10.1016/B978-0-08-099991-3.00004-1.

[17] N.H.N. Kamarudin, A.A. Jalil, S. Triwahyono, M.R. Sazegar, S. Hamdan, S. Baba, A. Ahmad, Elucidation of acid strength effect on ibuprofen adsorption and release by aluminated mesoporous silica nanoparticles, RSC Adv. 5 (2015) 30023–30031. doi:10.1039/C4RA16761A.

[18] Y. Choudhari, H. Hoefer, C. Libanati, F. Monsuur, W. McCarthy, Mesoporous Silica Drug Delivery Systems, in: N. Shah, H. Sandhu, D.S. Choi, H. Chokshi, A.W. Malick (Eds.), Amorph. Solid Dispersions Theory Pract., Springer New York, New York, NY, 2014: pp. 665–693. doi:10.1007/978-1-4939-1598-9_23.

[19] X. Guo, J. Wu, Y.-M. Yiu, Y. Hu, Y.-J. Zhu, T.-K. Sham, Drug-nanocarrier interaction-tracking the local structure of calcium silicate upon ibuprofen loading with X-ray absorption near edge structure (XANES), Phys. Chem. Chem. Phys. 15 (2013) 15033–15040. doi:10.1039/C3CP50699A.

[20] S. Wang, Ordered mesoporous materials for drug delivery, Microporous Mesoporous Mater. 117 (2009) 1–9. doi:http://dx.doi.org/10.1016/j.micromeso.2008.07.002.

[21] M. Manzano, V. Aina, C.O. Arean, F. Balas, V. Cauda, M. Colilla, M.R. Delgado, M. Vallet-Regí, Studies on MCM-41 mesoporous silica for drug delivery: Effect of particle morphology and amine functionalization, Chem. Eng. J. 137 (2008) 30–37. doi:10.1016/j.cej.2007.07.078.

[22] E.-P. Ng, J.-Y. Goh, T.C. Ling, R.R. Mukti, Eco-friendly synthesis for MCM-41 nanoporous materials using the non-reacted reagents in mother liquor., Nanoscale Res. Lett. 8 (2013) 120. doi:10.1186/1556-276X-8-120.

[23] T. Heikkilä, H.A. Santos, N. Kumar, D.Y. Murzin, J. Salonen, T. Laaksonen, L. Peltonen, J. Hirvonen, V.P. Lehto, Cytotoxicity study of ordered mesoporous silica MCM-41 and SBA-15 microparticles on Caco-2 cells, Eur. J. Pharm. Biopharm. 74 (2010) 483–494. doi:10.1016/j.ejpb.2009.12.006.

[24] X. Wang, P. Liu, Y. Tian, Ordered mesoporous carbons for ibuprofen drug loading and release behavior, Microporous Mesoporous Mater. 142 (2011) 334–340. doi:10.1016/j.micromeso.2010.12.018.

[25] Y. Zhang, Z. Zhi, X. Li, J. Gao, Y. Song, Carboxylated mesoporous carbon microparticles as new approach to improve the oral bioavailability of poorly water-soluble carvedilol, Int. J. Pharm. 454 (2013) 403–411. doi:10.1016/j.ijpharm.2013.07.009.

[26] Y. Zhang, H. Wang, C. Gao, X. Li, L. Li, Highly ordered mesoporous carbon nanomatrix as a new approach to improve the oral absorption of the water-insoluble drug, simvastatin, Eur. J. Pharm. Sci. 49 (2013) 864–872. doi:10.1016/j.ejps.2013.05.031.

[27] P. Zhao, L. Wang, C. Sun, T. Jiang, J. Zhang, Q. Zhang, J. Sun, Y. Deng, S. Wang, Uniform mesoporous carbon as a carrier for poorly water soluble drug and its cytotoxicity study, Eur. J. Pharm. Biopharm. 80 (2012) 535–543. doi:10.1016/j.ejpb.2011.12.002.

[28] H. Marsh, F. Rodriguez-reinoso, Activated Carbon, Technology. 94 (2006) 536. doi:10.1016/0160-9327(81)90123-X.

[29] M. Inagaki, Pores in carbon materials-importance of their control, New Carbon Mater. 24 (2009) 193–232.

[30] P. Liang, L. Yuan, X. Yang, S. Zhou, X. Huang, Coupling ion-exchangers with inexpensive activated carbon fiber electrodes to enhance the performance of capacitive deionization cells for domestic wastewater desalination, Water Res. 47 (2013) 2523–2530. doi:http://dx.doi.org/10.1016/j.watres.2013.02.037.

[31] K.R. Olson, Activated Charcoal for Acute Poisoning: One Toxicologist's Journey, J. Med. Toxicol. 6 (2010) 190–198. doi:10.1007/s13181-010-0046-1.

[32] D.N. Juurlink, Activated charcoal for acute overdose: A reappraisal, Br. J. Clin. Pharmacol. 81 (2016) 482–487. doi:10.1111/bcp.12793.

[33] F. Guo, X. Mao, J. Wang, F. Luo, Z. Wang, Gemcitabine adsorbed onto carbon particles increases drug concentrations at the injection site and in the regional lymph nodes in an animal experiment and a clinical study, J. Int. Med. Res. 39 (2011) 2119–2127. doi:10.1177/147323001103900618.

[34] C.F. Linares, A. Palencia, M.R. Goldwasser, K. Rodríguez, Study of activated carbon modified with sodium carbonate as a possible antacid drug, Mater. Lett. 60 (2006) 439–441. doi:10.1016/j.matlet.2005.09.020.

[35] C.F. Linares, J. Quintero, L. Mart??nez, G. Gonz??lez, A new antacid drug from activated carbon modified with calcium carbonate, Mater. Lett. 61 (2007) 2362–2364. doi:10.1016/j.matlet.2006.09.012.

[36] M. Chu, J. Peng, J. Zhao, S. Liang, Y. Shao, Q. Wu, Laser light triggered-activated carbon nanosystem for cancer therapy, Biomaterials. 34 (2013) 1820–1832. doi:http://dx.doi.org/10.1016/j.biomaterials.2012.11.027.

[37] T. Yokota, T. Saito, Y. Narushima, K. Iwamoto, M. Iizuka, A. Hagiwara, K. Sawai, S. Kikuchi, Y. Kunii, H. Yamauchi, Lymph-node staining with activated carbon CH40: A new method for axillary lymph-node dissection in breast cancer, Can. J. Surg. 43 (2000) 191–196. https://www.scopus.com/inward/record.uri?eid=2-s2.0-0034121759&partnerID=40&md5=bc26703328c5631cfcc16e8e97fbc6f8.

[38] J. Yun, J.S. Im, D. Jin, Y.-S. Lee, H.-I. Kim, Controlled release behavior of temperature responsive composite hydrogel containing activated carbon, Carbon Lett. 9 (2008) 283–288.

[39] J. Salonen, J. Paski, K. Vähä-Heikkilä, T. Heikkilä, M. Björkqvist, V.-P. Lehto, Determination of drug load in porous silicon microparticles by calorimetry, Phys. Status Solidi. 202 (2005) 1629–1633. doi:10.1002/pssa.200461204.

[40] R.A. Granberg, Å.C. Rasmuson, Solubility of Paracetamol in Pure Solvents, J. Chem. Eng. Data. 44 (1999) 1391–1395. doi:10.1021/je990124v.

[41] S. Gracin, Å.C. Rasmuson, Solubility of Phenylacetic Acid, p-Hydroxyphenylacetic Acid, p-Aminophenylacetic Acid, p-Hydroxybenzoic Acid, and Ibuprofen in Pure Solvents, J. Chem. Eng. Data. 47 (2002) 1379–1383. doi:10.1021/je0255170.

[42] Y. Kong, J.N. Hay, The measurement of the crystallinity of polymers by DSC, Polymer (Guildf). 43 (2002) 3873–3878. doi:http://dx.doi.org/10.1016/S0032-3861(02)00235-5.

[43] Y. Zhang, H. Wang, C. Li, B. Sun, Y. Wang, S. Wang, C. Gao, A novel three-dimensional large-

pore mesoporous carbon matrix as a potential nanovehicle for the fast release of the poorly water-soluble drug, celecoxib, Pharm. Res. 31 (2014) 1059–1070. doi:10.1007/s11095-013-1227-9.

[44] M.P. Desai, V. Labhasetwar, E. Walter, R.J. Levy, G.L. Amidon, The Mechanism of Uptake of Biodegradable Microparticles in Caco-2 Cells Is Size Dependent, Pharm. Res. 14 (1997) 1568–1573. doi:10.1023/A:1012126301290.

[45] Y. He, K. Park, Effects of the microparticle shape on cellular uptake, Mol. Pharm. 13 (2016) 2164–2171. doi:10.1021/acs.molpharmaceut.5b00992.

[46] E. Fröhlich, The role of surface charge in cellular uptake and cytotoxicity of medical nanoparticles, Int. J. Nanomedicine. 7 (2012) 5577–5591. doi:10.2147/IJN.S36111.

[47] A. Baeza-Squiban, G. Lacroix, F.Y. Bois, Experimental Models in Nanotoxicology, in: P. Houdy, M. Lahmani, F. Marano (Eds.), Nanoethics and Nanotoxicology, Springer Berlin Heidelberg, Berlin, Heidelberg, 2011: pp. 63–86. doi:10.1007/978-3-642-20177-6_3.

[48] S. Qi, P. Avalle, R. Saklatvala, D.Q.M. Craig, An investigation into the effects of thermal history on the crystallisation behaviour of amorphous paracetamol, Eur. J. Pharm. Biopharm. 69 (2008) 364–371. doi:http://dx.doi.org/10.1016/j.ejpb.2007.10.008.

[49] H. Cano, N. Gabas, J.P. Canselier, Experimental study on the ibuprofen crystal growth morphology in solution, J. Cryst. Growth. 224 (2001) 335–341. doi:http://dx.doi.org/10.1016/S0022-0248(01)00969-1.

[50] F. Xu, L.-X. Sun, Z.-C. Tan, J.-G. Liang, R.-L. Li, Thermodynamic study of ibuprofen by adiabatic calorimetry and thermal analysis, Thermochim. Acta. 412 (2004) 33–57. doi:http://dx.doi.org/10.1016/j.tca.2003.08.021.

[51] C. Wang, L. Feng, H. Yang, G. Xin, W. Li, J. Zheng, W. Tian, X. Li, Graphene oxide stabilized polyethylene glycol for heat storage, Phys. Chem. Chem. Phys. 14 (2012) 13233–13238. doi:10.1039/C2CP41988B.

[52] L. Chen, R. Zou, W. Xia, Z. Liu, Y. Shang, J. Zhu, Y. Wang, J. Lin, D. Xia, A. Cao, Electro- and Photodriven Phase Change Composites Based on Wax-Infiltrated Carbon Nanotube Sponges, ACS Nano. 6 (2012) 10884–10892. doi:10.1021/nn304310n.

[53] Y. Liu, K. Yan, G. Jiang, Y. Xiong, Y. Du, X. Shi, Electrical Signal Guided Ibuprofen Release from Electrodeposited Chitosan Hydrogel, Int. J. Polym. Sci. 2014 (2014) 8. doi:10.1155/2014/736898.

[54] Á. Martín, K. Scholle, F. Mattea, D. Meterc, M.J. Cocero, Production of Polymorphs of Ibuprofen Sodium by Supercritical Antisolvent (SAS) Precipitation, Cryst. Growth Des. 9 (2009) 2504–2511. doi:10.1021/cg900003m.

[55] I.-C. Wang, M.-J. Lee, D.-Y. Seo, H.-E. Lee, Y. Choi, W.-S. Kim, C.-S. Kim, M.-Y. Jeong, G.J. Choi, Polymorph Transformation in Paracetamol Monitored by In-line NIR Spectroscopy During a Cooling Crystallization Process, AAPS PharmSciTech. 12 (2011) 764–770. doi:10.1208/s12249-011-9642-x.

[56] P. Wilhelm, Applications of FT-IR microscopy with materials analyses, Micron. 27 (1996) 341–344. doi:10.1016/S0968-4328(96)00020-0.

[57] S.G. Kazarian, K.L.A. Chan, ATR-FTIR spectroscopic imaging: recent advances and applications to biological systems., Analyst. 138 (2013) 1940–51. doi:10.1039/c3an36865c.

[58] S. Chen, J. Zhang, C. Zhang, Q. Yue, Y. Li, C. Li, Equilibrium and kinetic studies of methyl orange and methyl violet adsorption on activated carbon derived from Phragmites australis, Desalination. 252 (2010) 149–156. doi:http://dx.doi.org/10.1016/j.desal.2009.10.010.

Figures

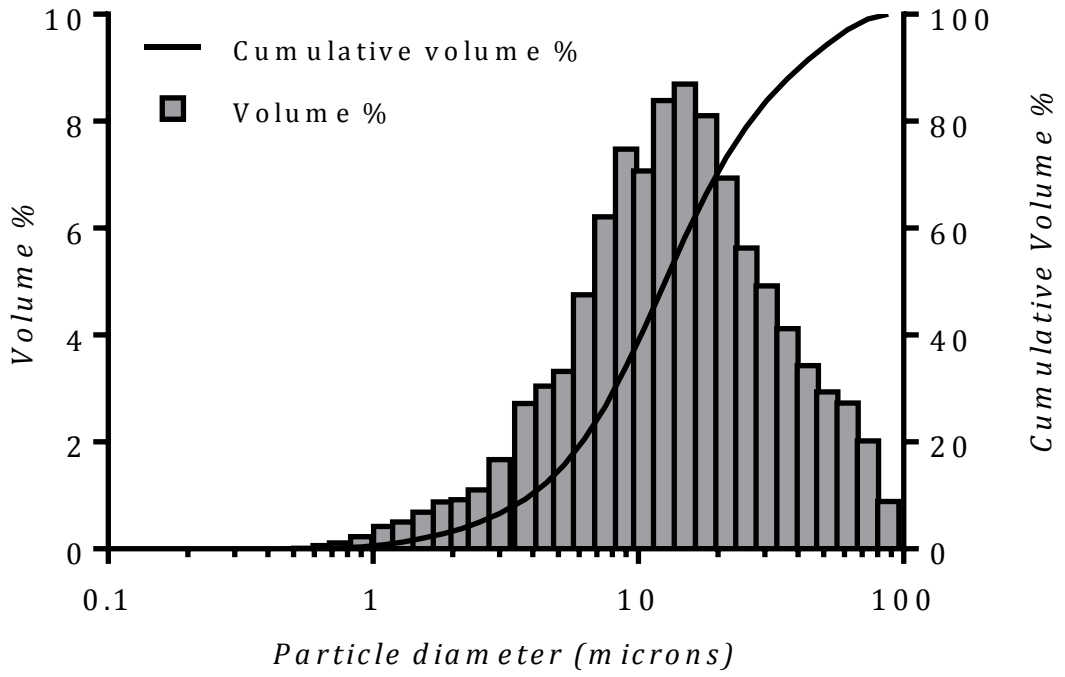

Material	X90[a] (µm)	X50[b] (µm)	X10[c] (µm)	Volume mean diameter (µm)	Span
Activated carbon	40.59 ± 0.53	12.62 ± 0.09	3.92 ± 0.02	17.85 ± 0.15	2.91 ± 0.02

[a] Particle dimension corresponding to 90% of the cumulative undersize distribution

[b] Median particle dimension

[c] Particle dimension corresponding to 10% of the cumulative undersize distribution

Fig. 1. Particle size distribution of activated carbon obtained from laser diffraction.

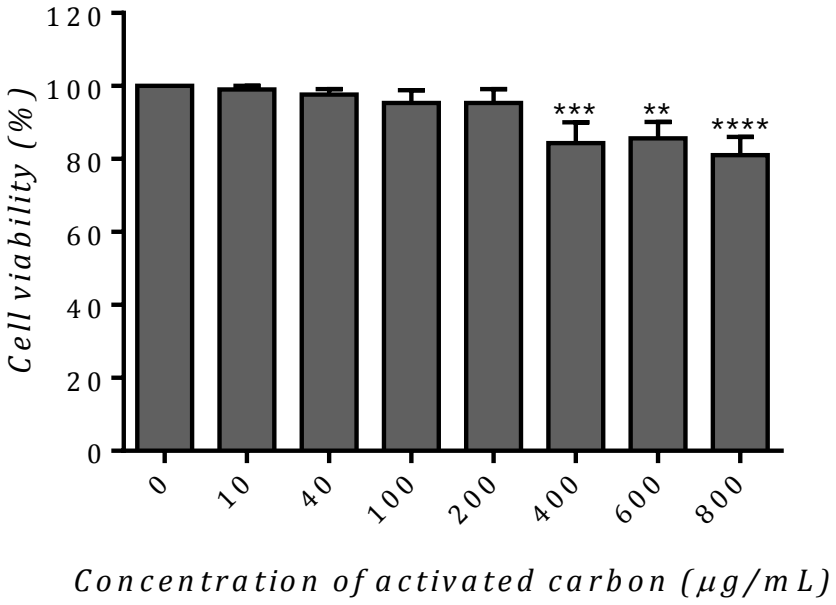

Fig. 2. Cytotoxicity of activated carbon against Caco-2 cells. MTT assay was used to analyse the survival rate of Caco-2 cells incubated with different concentrartions of activated carbon. Statistically significant differences compared to control (0 µg/mL) are noted for $P < 0.05$ ($^{*}P \leq 0.05$; ** $P \leq 0.01$; *** $P \leq 0.001$; **** $P \leq 0.0001$, one way ANOVA and Dunnett's multiple comparison test).

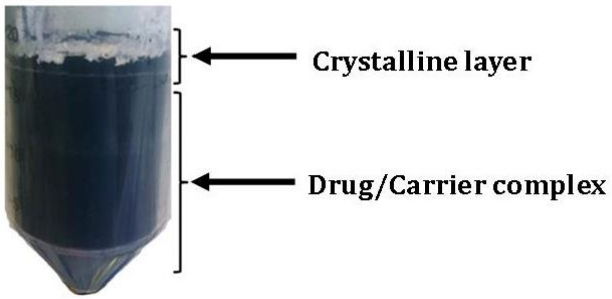

Fig. 3: Photographic image of drug/carrier complex and crystallised drug obtained after drying the sediment obtained from centrifugation. Top white crystalline layer is separated and the bottom layer is considered as drug/Carrier complex for further analysis.

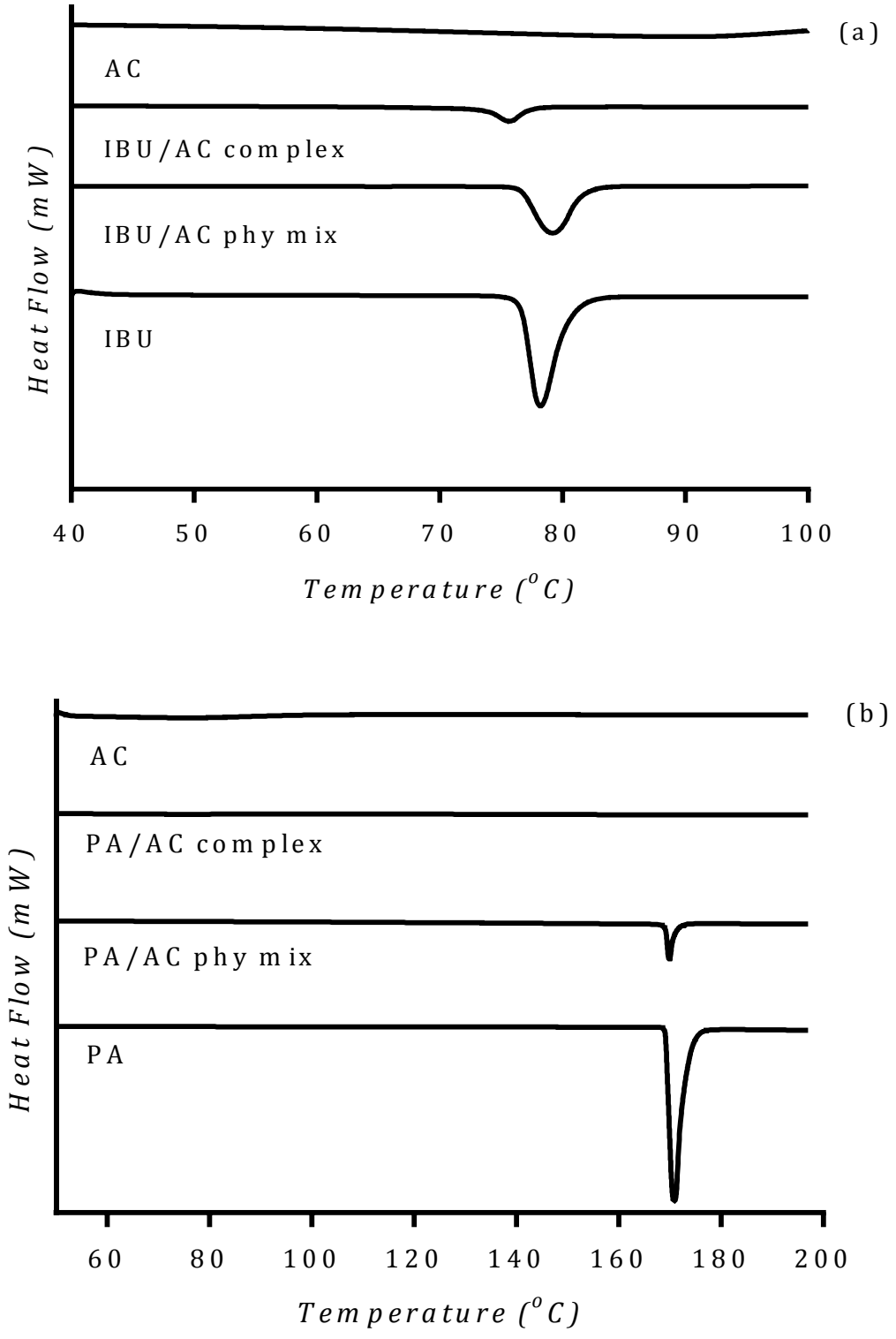

Fig. 4: DSC curves of (a) pure ibuprofen (IBU), pure activated carbon (AC), ibuprofen loaded activated carbon sample (IBU/AC complex) and physical mixture of ibuprofen and activated carbon (IBU/AC phy mix) (b) pure paracetamol (PA), pure activated carbon (AC), paracetamol loaded activated carbon sample (PA/AC complex) and physical mixture of paracetamol and activated carbon (PA/AC phy mix).

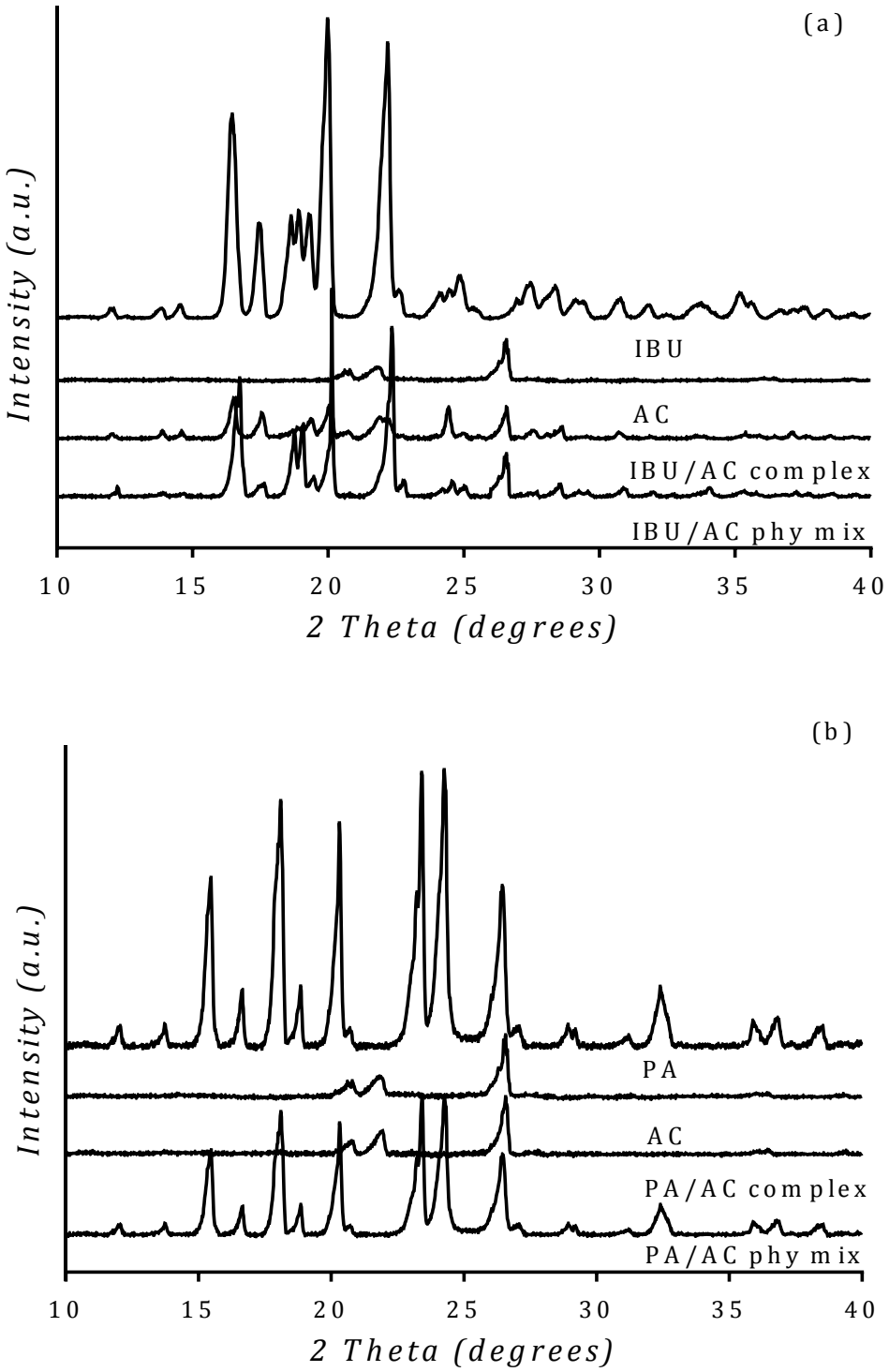

Fig. 5: XRD patterns of (a) pure ibuprofen (IBU), pure activated carbon (AC), ibuprofen loaded activated carbon sample (IBU/AC complex) and physical mixture of ibuprofen and activated carbon (IBU/AC phy mix) (b) pure paracetamol (PA), pure activated carbon (AC), paracetamol loaded activated carbon sample (PA/AC complex) and physical mixture of paracetamol and activated carbon (PA/AC phy mix).

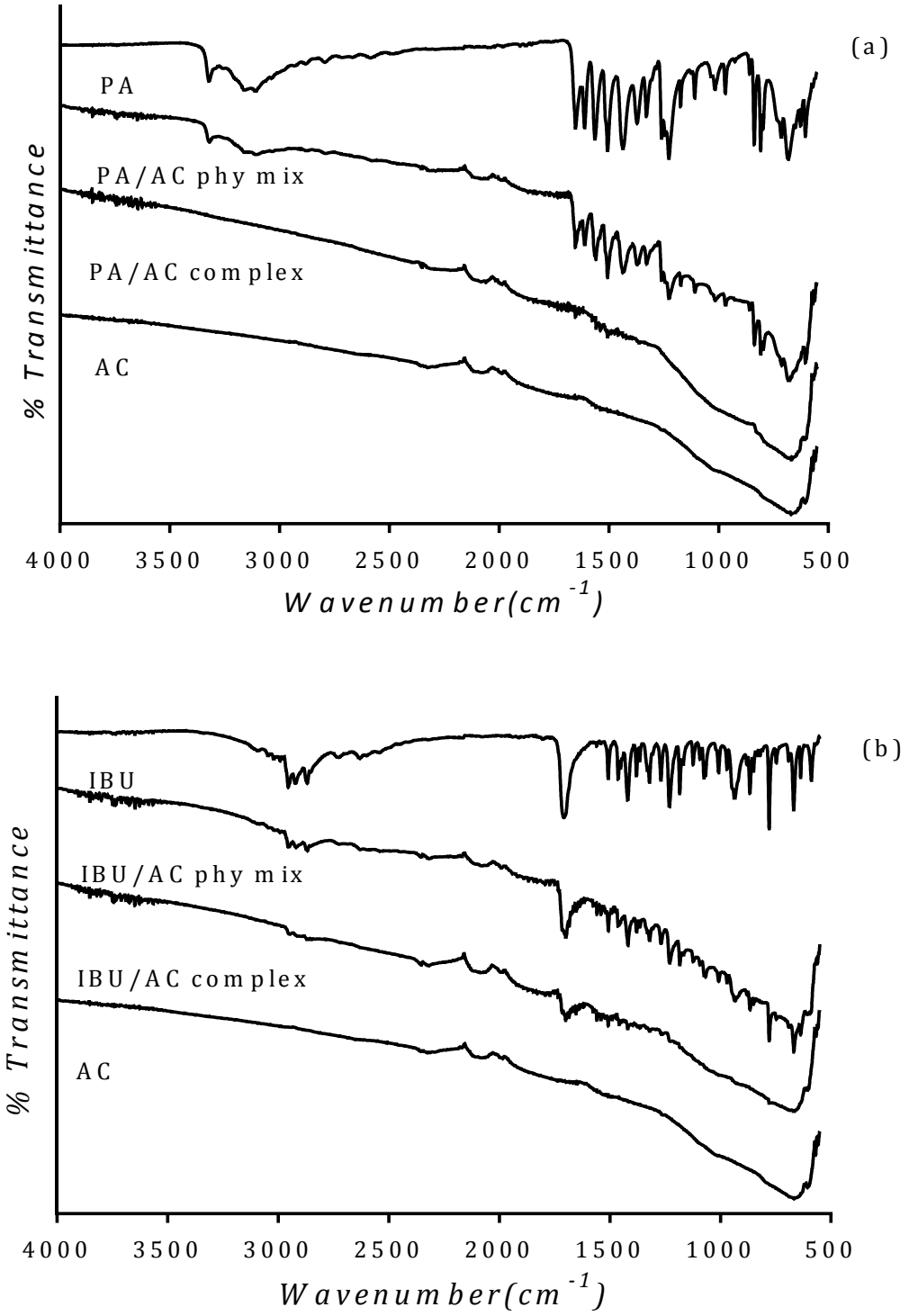

Fig. 6: FTIR spectra of (a) pure paracetamol (PA), pure activated carbon (AC), paracetamol loaded activated carbon sample (PA/AC complex) and physical mixture of paracetamol and activated carbon (PA/AC phy mix) (b) pure ibuprofen (IBU), pure activated carbon (AC), ibuprofen loaded activated carbon sample (IBU/AC complex) and physical mixture of ibuprofen and activated carbon (IBU/AC phy mix).

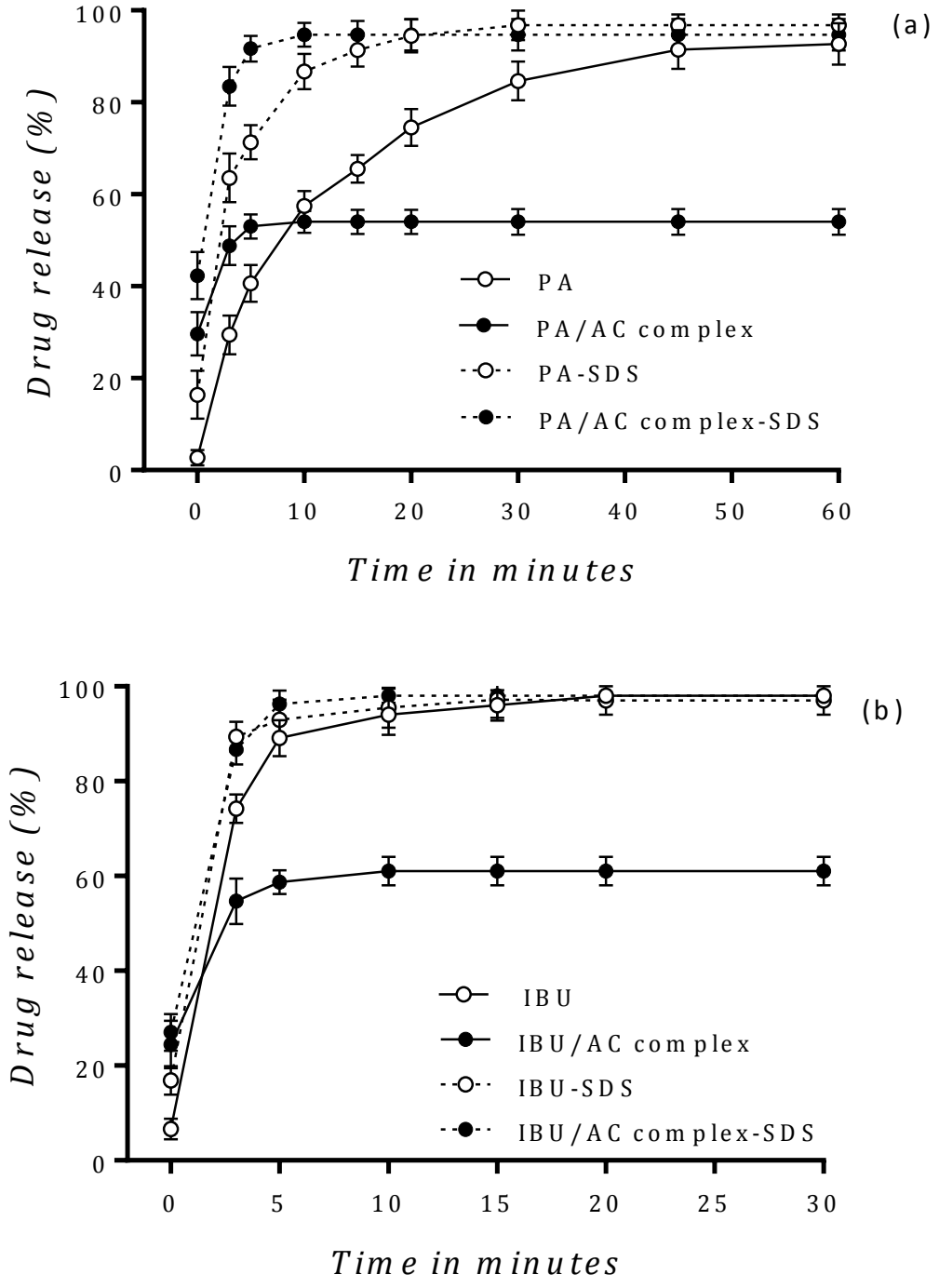

Fig. 7: Comparison of cumulative drug release from pure drug and drug loaded carrier samples at 37°C using paddle type dissolution apparatus. (a) Curves PA and PA/AC complex represent pure paracetamol and paracetamol loaded activated carbon samples in sodium phosphate buffer (pH 5.8). Curves PA-SDS and PA/AC complex-SDS represents pure paracetamol and paracetamol loaded activated carbon samples in sodium phosphate buffer (pH 5.8) containing 1% SDS. (b) Curves IBU and IBU/AC complex represent pure ibuprofen and ibuprofen loaded activated carbon samples in sodium phosphate buffer (pH 7.2). Curves IBU-SDS and IBU/AC complex-SDS

represent pure ibuprofen and ibuprofen loaded activated carbon samples in sodium phosphate buffer (pH 7.2) containing 1% SDS.

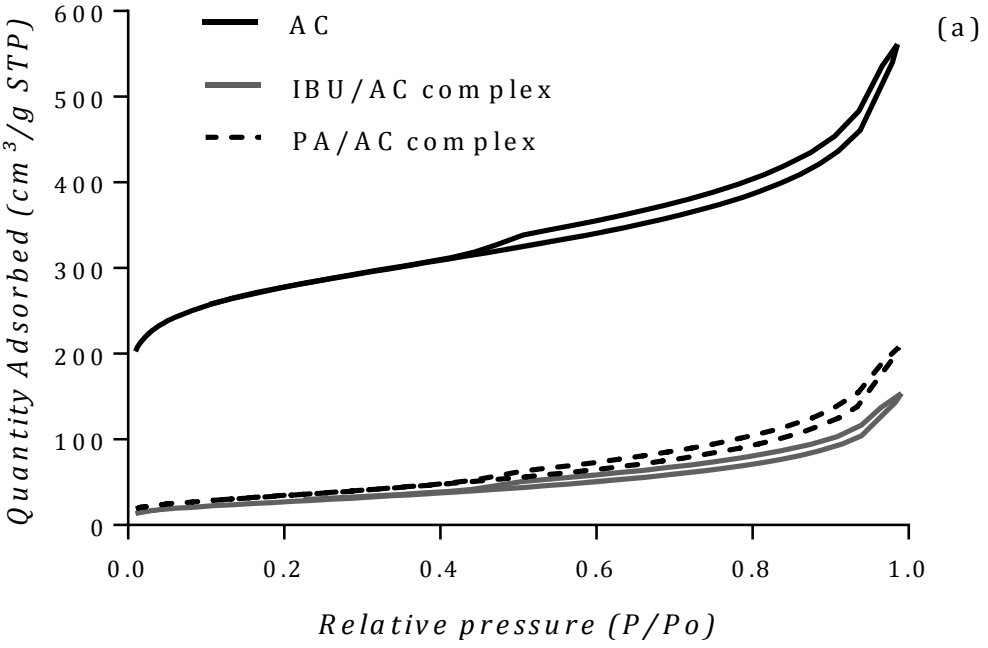

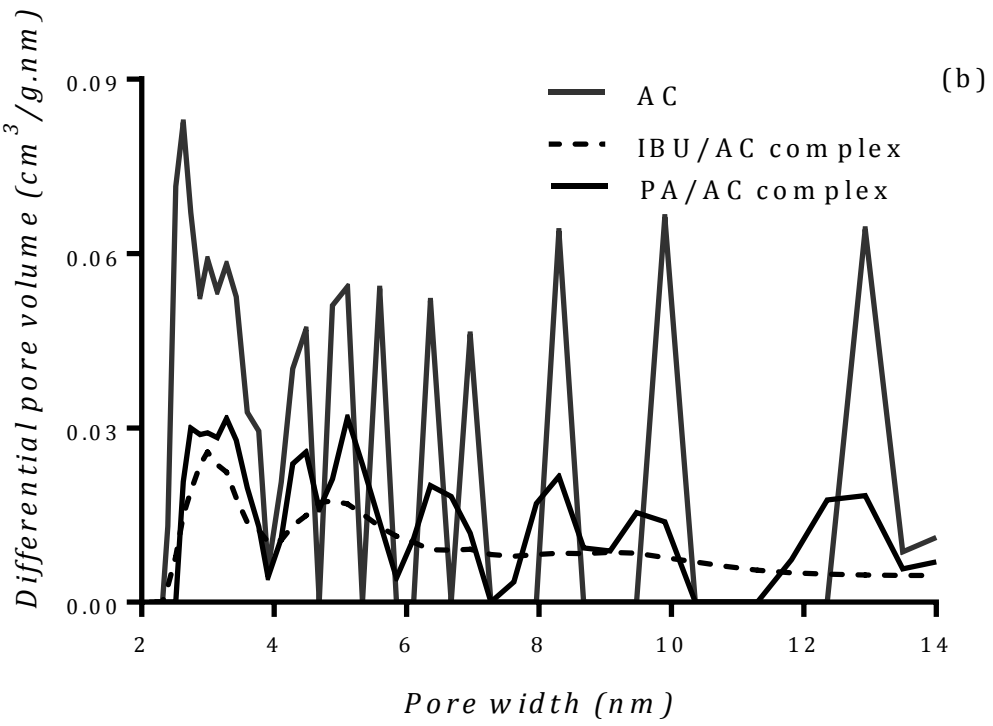

Fig. 8: (a) Nitrogen adsorption/desorption isotherms at 77 K (b) Pore size distribution (2-14nm) calculated using NLDFT-slit shaped pore model, of pure activated carbon (AC), ibuprofen loaded activated carbon (IBU/AC complex) and paracetamol loaded activated carbon (PA/AC complex).

Tables

Table 1: Porous materials studied as carriers for amorphous drug delivery

Porous material	Surface area	Synthesis	Advantages	Limitations	Reference
Porous silicon	Up to 1000 m^2/g	Electrochemical etching	Biodegradable Ease of synthesis Ease of fabrication	Undergoes atmospheric oxidation Requires surface modification for stability Possible chemical interactions with drugs	[10–13]
Non ordered porous silica	Up to 800 m^2/g	Sol-gel process	Ease of synthesis	Surface silanol groups can chemically interact with carboxyl groups of drugs via hydrogen bonding or esterification and can pose risk of irreversible drug adsorption or slower drug release, which can be disadvantageous if immediate release is preferred Siloxane bridges might undergo hydrolysis	[12,14–19]
Ordered mesoporous silica (OMS)	Up to 1200 m^2/g	Surfactant templating	Uniform porosity Large surface area	Complicated and expensive synthesis Variable Toxicity results Chemical interactions between surface silanol groups and drugs, as with non ordered porous silica Siloxane bridges might undergo hydrolysis	[12,20–23]
Ordered mesoporous carbon	Up to 1400 m^2/g	Hard templating method	Uniform porosity Large surface area Chemically Inert Insoluble in biological fluids	Synthesis involves use of OMS as template Poor wettability	[24–27]

Table 2: Potential clinical applications of activated carbon

Potential applications	Result	Reference
Chemotherapy	Drugs adsorbed on to AC nano particles were selectively delivered to regional lymph nodes and retained at the site of injection for a longer duration in rats and cancer patients.	[33]
Antacid	Calcium carbonate or sodium carbonate adsorbed on the activated carbon was able to maintain ideal pH and neutralize gastric acidity without any rebound effect *in vitro*.	[34,35]
Photo thermal cancer therapy	When exposed to laser radiation, PVP dispersed AC nano particles were able to convert light in to heat energy and resulted in tumour growth suppression at the site of injection in mice.	[36]
Lymph node staining	AC of particle size < 200 nm injected was readily absorbed in to regional lymphatics and blackened lymph nodes.	[37]
Controlled release	AC containing temperature responsive hydrogel was used to increase the drug loading capacity and mechanical strength of the hydrogel for controlled release.	[38]

Table 3: Comparison of ibuprofen and paracetamol loading in activated carbon

Drug	Initial quantity of drug [a] (mg)	Quantity of drug in complex (mg)	% Loading efficiency	Quantity of drug in (mg)	
				Supernatant [b]	Crystalline layer [c]
PA	1500	208 ± 12.5	20.7 ± 1	985.5 ± 12	320.5 ± 6
IBU	6900	643 ± 77.7	44.4 ± 4	5592.4 ± 159	662.3 ± 174

[a] per 10 mL of Ethanol

[b] obtained from centrifugation

[c] top crystalline layer of the sediment after drying.

Table 4: Melting Enthalpy and Melting points obtained from differential scanning calorimetry of pure ibuprofen (IBU), pure activated carbon (AC), ibuprofen loaded activated carbon sample (IBU/AC complex) and physical mixture of ibuprofen and activated carbon (IBU/AC phy mix), pure paracetamol (PA), paracetamol loaded activated carbon sample (PA/AC complex) and physical mixture of paracetamol and activated carbon (PA/AC phy mix).

Sample	Drug carrier ratio (*w/w*)	Melting Enthalpy (J/g)	Melting temperature (°C)	% Crystallinity
IBU	1:0	130.3	74.8	100
IBU/AC phy mix	0.8:1	83.4	74.8	100
IBU/AC complex	0.8:1	15.78	72	19
PA	1:0	181	169.2	100
PA/AC phy mix	0.25:1	27.1	169.2	100
PA/AC complex	0.25:1	-	-	0

Table 5: Surface areas and pore volumes obtained from Nitrogen sorption of pure activated carbon (AC), ibuprofen loaded activated carbon (IBU/AC complex) and paracetamol loaded activated carbon (PA/AC complex)

Sample	Specific surface area[a] (m^2/g)	Total pore volume [b] (cm^3/g)	Micro pore volume [b] (cm^3/g)
AC	1027.4	0.81	0.33
PA/AC complex	127	0.31	0.016
IBU/AC complex	101.8	0.23	0.014

[a] Calculated by BET method

[b] Calculated by NLDFT method